The LINNEAN SOCIETY of London BIOLOGICAL Journal of the Linnean Society

Biological Journal of the Linnean Society, 2012, **106**, 224–240. With 10 figures

Exploring feeding behaviour in deep-sea dragonfishes (Teleostei: Stomiidae): jaw biomechanics and functional significance of a loosejaw

CHRISTOPHER P. KENALEY*

School of Aquatic and Fishery Sciences, Burke Museum of Natural History and Culture, University of Washington, Seattle, WA 98195, USA

Received 3 June 2011; revised 30 November 2011; accepted for publication 30 November 2011

Deep-sea dragonfishes (family Stomiidae) possess spectacular morphologies adapted to capturing large prey items in a seascape largely devoid of biomass, including large fang-like teeth set on extremely long jaws. Perhaps the most intriguing aspect of dragonfish morphology is a lack of a floor to the oral cavity (i.e. there is no skin between the mandibular rami) in species of three dragonfish genera. The present study aimed to investigate the kinematic properties and performance of lower-jaw adduction in stomiid fishes and to infer what functional advantages or constraints the 'loosejaw' confers. A computation model based on dynamic equilibrium predicted very fast jaw adduction for all species at gapes ranging from 90–120° in 66.6–103 ms. Simulations demonstrated that forces resisting lower-jaw adduction in dragonfishes, and long-jawed fishes in general, are substantially greater than those in fishes with shorter jaws. These forces constrain inlever length, resulting in relatively high mechanical advantages to attain fast adduction velocities. By reducing the surface area of the lower-jaw system, loosejaws drastically reduce resistive forces. This has permitted loosejaw dragonfishes to evolve lower mechanical advantages that produce high displacement velocities with an extremely long jaw, a distinct asset in capturing large and scarce resources in the deep-sea. In addition, loosejaws require a substantially reduced adductor mass to close long jaws at high velocities. These results reveal that the loosejaw condition is an adaptation that expands the morphological boundaries imposed by the dynamic limitations of a long jaw. *Biological Journal of the Linnean Society*, 2012, **106**, 224–240.

ADDITIONAL KEYWORDS: computer simulation – dynamic-equilibrium model – mechanical advantage – morphology.

INTRODUCTION

Fishes of the teleost family Stomiidae, the dragonfishes, sit atop deep-sea pelagic food webs, consuming as much as an estimated 58–230% of the annual standing stock of their prey, typically smaller myctophiform and gonostomatid fishes (Clarke, 1982; Sutton & Hopkins, 1996). As apex predators, stomiid fishes possess enormous jaws laden with fang-like teeth and, as a result of occipito-vertebral reduction or gaps in many species (Schnell, Britz & Johnson, 2010), also the ability to hinge the neurocranium and upper-jaw system and thus open the jaw to gape angles greater than 100° (Fig. 1A) (Tchernavin, 1953; Günther & Deckert, 1959). In addition, jaw lengths of many stomiid species approach 20% of standard length, which is several times longer than the neurocranium. These enormous jaws and wide gapes enable dragonfishes to consume extremely large prey items that are often greater than 50% their standard lengths (Clarke, 1982; Sutton & Hopkins, 1996).

The genera *Aristostomias* Zugmayer, *Malacosteus* Ayres, *Photostomias* Collett, and *Pachystomias* Günther, differ substantially from other stomiid genera in having jaw lengths greater than 30% their standard length (Kenaley & Hartel, 2005; Kenaley, 2007, 2009; C. Kenaley, unpubl. data) and possessing at least one accessory orbital photophore (AO). *Aristostomias, Malacosteus*, and *Pachystomias*

*Corresponding author. E-mail: ckenaley@uw.edu

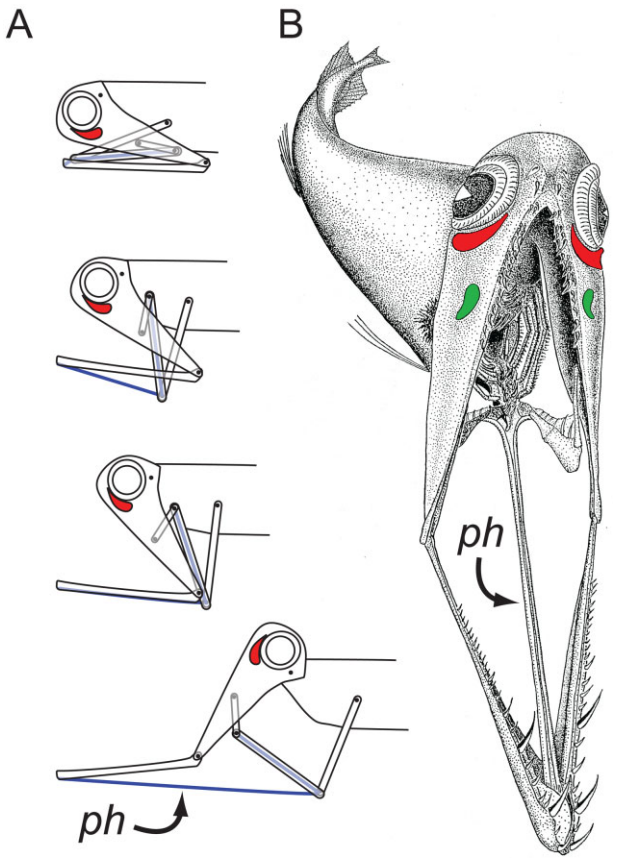

Figure 1. A, schmatic representing the linkages that form the feeding position of dragonfishes and utilization of the occipital-vertebral hinge to create high gape angles. B, head-on view of *Malacosteus niger*, demonstrating its hypothesized feeding position (*sensu* Günther & Deckert, 1959). *ph*, protractor hyoideus.

are unique among vertebrates in their ability to produce long-wave bioluminescence, their AOs producing emission maxima greater than 525 nm (Partridge & Douglas, 1995; Douglas *et al*., 1999; Hunt *et al*., 2001). Perhaps the most striking feature of these fishes is (except for a small symphyseal membrane) the absence of skin between the mandibular rami in species of the genera *Aristostomias, Malacosteus*, and *Photostomias* (Figs 1B, 2). In their classic study of the functional morphology of *Malacosteus* and *Photostomias*, Günther & Deckert (1959) proposed that the the 'loosejaw' is depressed by the protractor hyoideus, whereas the upper-jaw system and neurocranium are rotated forward on the hinge of the occipito-vertebral gap. This creates a trap of sorts set around an extremely wide gape (> 120°) that, through the absence of an interandibular membrane, would be shut rapdily against a prey item (Fig. 1). As proposed by Partridge & Douglas (1995), the far-red field cast by the AO covertly illuminates the prey item, allowing the loosejaw to detect its target and spring the trap.

The present study aimed to investigate the feeding performance and biomechanical properties of species of four dragonfish genera, including two plesiomorphic species and two loosejaw species, and to infer what functional advantages or constraints the loosejaw morphology confers on these taxa. Specifically, the study addresses two open questions: (1) do the dynamics of feeding vary between relatively plesiomorphic and loosejaw species of dragonfishes and (2) in what way does the loosejaw condition affect the feeding performance of fishes that possess the morphology?

Because of the inherent difficulties associated with studying deep-sea taxa in the laboratory, questions such as these that focus on the functional morphology of deep-sea fishes (i.e. how morphology limits behaviour) have remained largely unexplored. Our current understanding of the relationship between morphology and feeding behaviour in oceanic, deep-sea taxa has been informed, in large part, by the dissection and manipulation of preserved specimens (Tchernavin, 1953; Günther & Deckert, 1959). Pietsch's (1978) prediction of suction-feeding performance in the tube-eye (*Stylephorus chordatus* Shaw) remains the only application of theoretical biomechanical models in a deep-sea vertebrate taxon. More recently, a modelling approach has proven valuable in the prediction of feeding performance and analysis of comparative biomechanics in other species unavailable for *in vivo* experimental analysis, namely fossil taxa (Anderson & Westneat, 2007; Kammerer, Grande & Westneat, 2006). Thus, the application of computational biomechanical models in the study of deep-sea fishes, although currently unutilized, may provide valuable insight into the behaviour of these taxa.

To address the two questions posed above, a computational biomechanical model was developed, based on a dynamic equilibrium in which the mass of the lower jaw was accelerated when the sum of positive forces (i.e. torque provided by the adductor mandibulae complex) overcomes forces known to resist jaw adduction, such as inertia, drag, and buccal pressure. This model is based on the attendant hydrodynamic and inertial properties of geometric shapes representing the lower-jaw system of dragonfishes, the dimensions of which were estimated with biometric data taken from preserved museum specimens.

MATERIAL AND METHODS

MORPHOLOGICAL DATA

The theoretical models implemented in jaw-closing simulations conformed to the morphological proper-

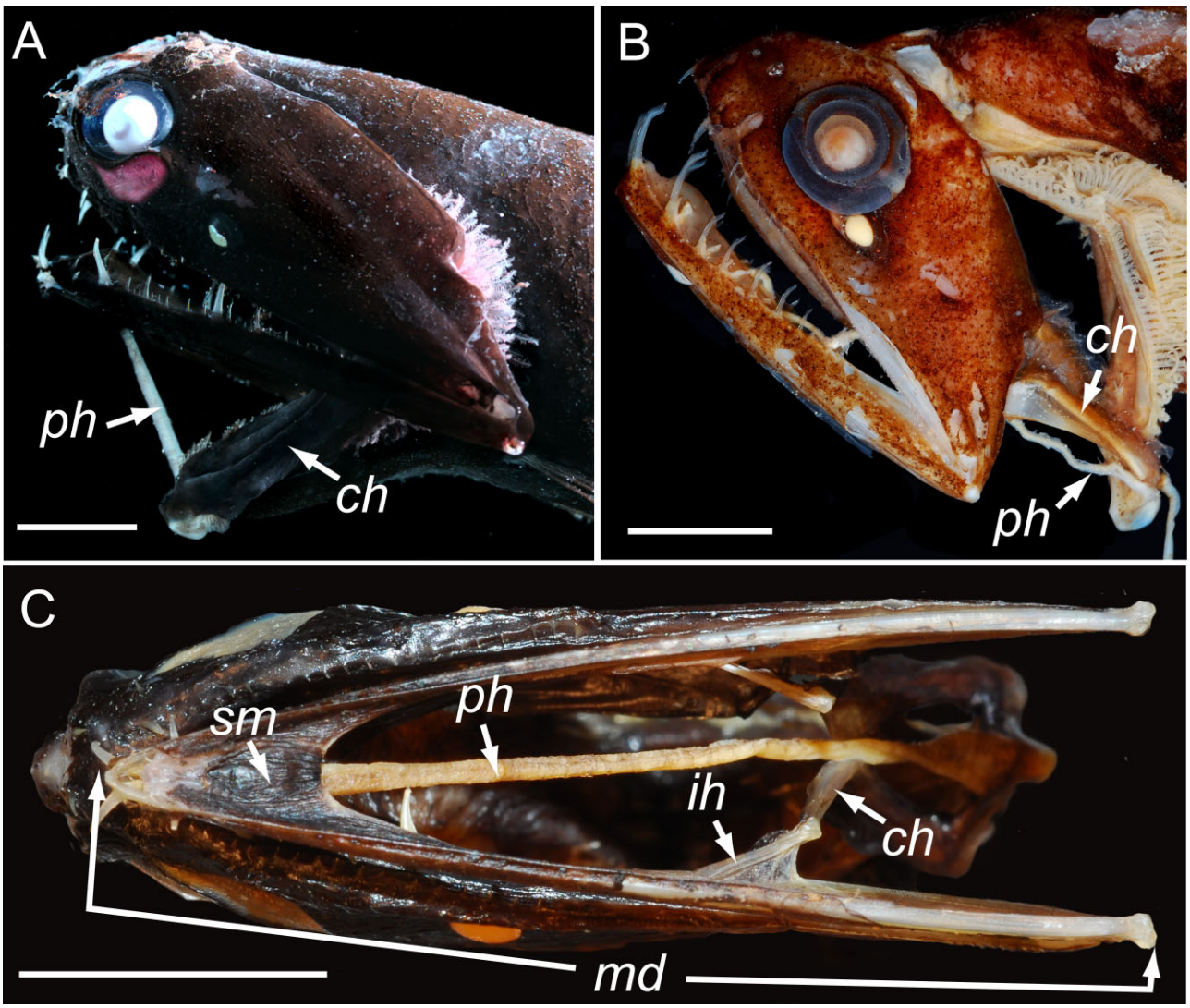

Figure 2. Two species of loosejaw dragonfishes modelled in the present study. A, *Malacosteus niger*, left lateral view of head. B, *Aristostomias scintillans*, left lateral view of head. C, ventral view of lower-jaw system and hyoid apparatus of *Malacosteus niger*. Note the lack of intermandibular membrane as indicated by the exposed protractor hyoideus muscle. *ph*, protractor hyoideus; *ch*, ceratohyal; *ih*, interhyal; *md*, mandible (i.e., articular + dentary); *sm*, syphyseal membrane. Scale bars in the lower left of each field represent 1 cm. The image in (A) is provided courtesy of E. Widder. Ocean Research & Conservation Association, Fort Pierce, FL.

ties of the oral-jaw system of two plesiomorphic stomiid species, *Chauliodus macouni* Bean and *Opostomias mitsuii* Imai (Fig. 3), and two loosejaw species, *Aristostomias scintillans* Gilbert and *Malacosteus niger* Ayres (Fig. 2). All morphological data required by the biomechanical model were taken from four specimens of each species (see 'Material examined' in the Supporting information, Appendix S1). To avoid the potentially confounding effect that ontogeny might have on jaw-closing performance, specimens with a lower-jaw length of approximately 30 mm were chosen for study. The dimensions of each morphological variable are indicated in Figure 4 and their values are recorded in the Supporting information (Table S1). With two exceptions, all morphological data were recorded from digital images taken of the right lateral side of the head of each specimen with the jaw closed. Lower-jaw length (L_j) was measured from the anteriormost point of the dentary to the posteriormost point of the articular. Outlever length (L_o) was measured from the quadrato-articular joint to the anteriormost point of the dentary. Inlever length (L_i) was measured from insertion of the adductor tendons to the quadrato-articular joint. Mandible width (M_w) and depth (D_m) were calculated as the average of these dimension based on ten mea-

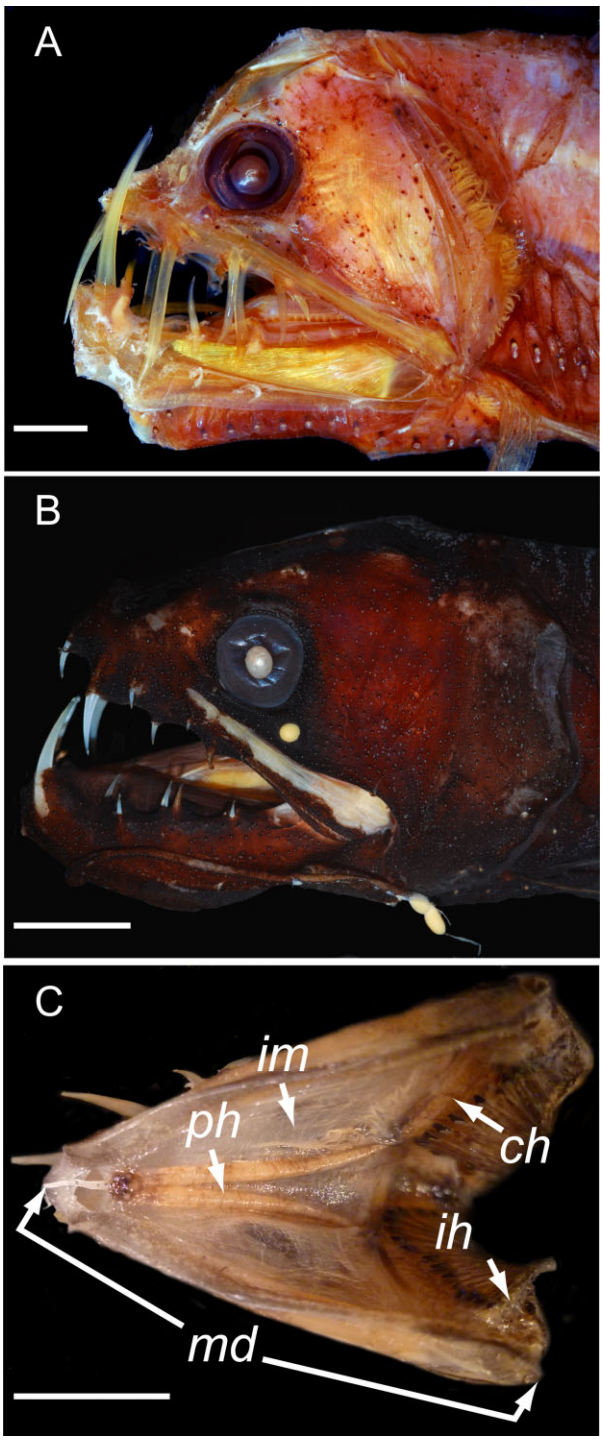

Figure 3. Two species of plesiomorphic dragonfishes, taxa with an intermandibular membrane present. A, *Chauliodus macouni*, left lateral view of head. B, *Opostomias mitsuii*, left lateral view of head. C, lower-jaw system and hyoid apparatus of *Chauliodus macouni*, ventral view. *ph*, protractor hyoideus; *ch*, ceratohyal; *ih*, interhyal; *im*, intermandibular membrane; *md*, mandible (i.e. articular + dentary). Scale bars in the lower left of each field represent 1 cm.

surements along the length of the lower jaw. The muscle origin–joint distance (D_{oj}) was measured from the centre of the adductor origin (inline with the central tendon in pennate segments) to the quadrato-articular joint. Gape angle (σ) was measured between L_o and a line through the upper jaw between the axis quadrato-articular joint and the most anterior point of the premaxilla. These data were subsequently processed in IMAGEJ (Rasband, 1997–2010). The width of the lower-jaw system at the quadrato-articular joint and mandibular width were measured with digital calipers. All other input parameters were calculated geometrically and represented below in the model description by lowercase notation (i.e. *a, l*, etc.).

Species of the genera modelled in the present study possess relatively simple jaw-closing systems with bones of the upper jaw fixed to the neurocranium (Fink, 1985). Therefore, the jaws are closed solely by rotation of the lower jaw at the quadrato-articular joint. In this scenario, the jaw-system acts as a simple third-order lever, with the muscles of the adductor mandibulae complex powering adduction at an attachment anterior to the fulcrum at the jaw joint (Westneat, 1994, 2003, 2004). Three sections of the adductor mandibulae complex power lower-jaw adduction in the four dragonfishes studied: the A2, A3, and Aω sections (Fig. 4A). Between the four species, the A3 section originates along the preopercle and lateral faces of the hyomandibula, symplectic, and metapterygoid. The A2 section originates on the posterior face of the sphenotic process, the pterotic, posterior ramus, and lateral face of the hyomandibula, and the preopercle. Both the A2 and A3 sections have tendinous insertions on the Meckelian fossa. The Aω section originates along the anteromedial face of the angular and attaches to the A2 tendon. In all species except *O. mitsuii*, the A2 division of the adductors is a fusiform, nonpennate muscle. For these sections, fibre length was calculated *sensu* Westneat (2003) by subtracting the tendon length from the distance of the A2 origin to its insertion on the Meckelian fossa. The Aω section of *A. scintillans* and *M. niger* is minute and was not included in muscle force calculations. The Aω section of *C. macouni* and *O. mitsuii* is substantial and, for specimens of these two genera, the mass of the Aω was added to the mass of the A2. After immersion in 2.0 M phosphate-buffered saline for 30 h, the adductor muscles were removed from the right side of each specimen, patted dry, and then weighed to the nearest 0.1 mg (see 'Muscle preparation' in the Supporting information, Appendix S1).

The average pennation (θ) angle for each pennated muscle segment was computed by measuring the angle between the muscle fibres and the central tendon at ten positions along the long axis of the

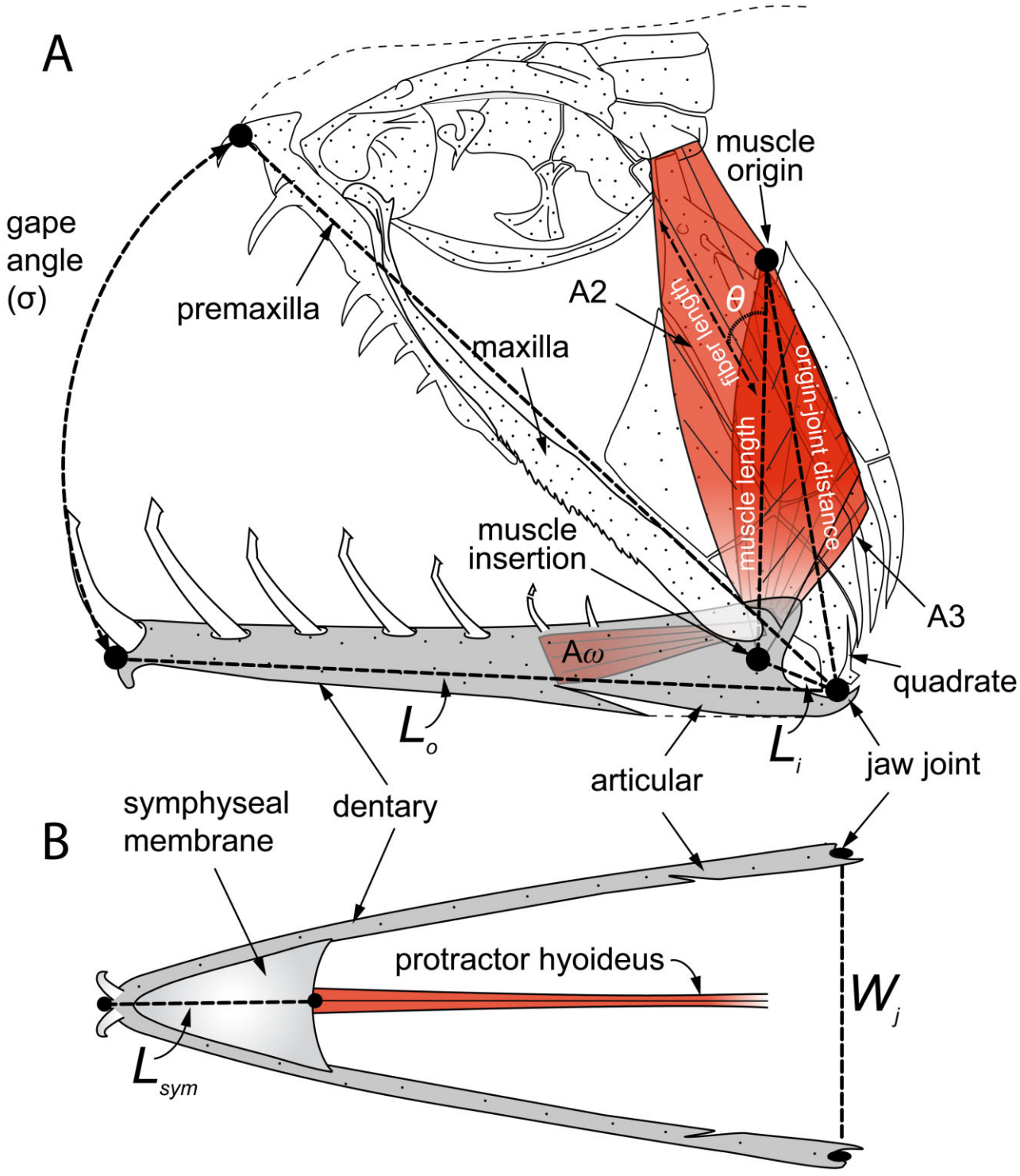

Figure 4. Schematic representation of variables of the lower-jaw lever system used in model calculations of bite force and jaw-adduction dynamics in four dragonfish species (Table 1); A, lateral view, B, ventral view. L_i, inlever length; L_o, outlever length; L_{sym}, length of symphyseal membrane; θ, muscle-fibre pennation angle.

segment. Average muscle-fibre length (*FL*) was similarly estimated by measuring the length of a fibre from its origin to attachment on the central tendon at the same ten points along the muscle (Fig. 4). Muscle and osteology nomenclature are based on previous studies by Winterbottom (1974) and Fink (1985), respectively.

Biomechanical model

Lower-jaw adduction was simulated using a dynamic equilibrium model based on that reported by Van Wassenbergh *et al*. (2005), a model developed for the jaw-lever system of clariid catfishes. Under this model, the mass component of the lower jaw will be accelerated when the sum of negative and positive torques is positive, a dynamic situation summarized by the equation:

$$\alpha = \frac{\tau_m + \tau_{dr} + \tau_{pr}}{I},$$

where α is the angular acceleration of the lower jaw in rad s^{-1}, I is the mass moment of inertia of the lower jaw and the water it puts into motion, and τ_m, τ_{dr}, and τ_{pr} are the torques applied by the jaw adductor muscles, drag, and pressure, respectively.

For the plesiomorphic *C. macouni* and *O. mitsuii*, species with skin between the mandibular rami, the lower jaw was modelled *sensu* Van Wassenbergh *et al*. (2005) with the exceptions outlined below (see also 'Model alterations' in the Supporting information, Appendix S1). This model approximates the mass properties of the lower-jaw system by modelling the lower jaw as a half ellipsoid of water rotating about the quadrato-articular joint. Pressure and drag torques were estimated according to the surface area of a half-elliptical plate with the same dimensions in the sagittal and coronal planes of the half ellipsoid representing the mass of the lower jaw.

For the loosejaw species *M. niger* and *A. scintillans*, the mass component of the lower jaw was modelled as the jaw itself and the mass of the water put into motion by the symphyseal membrane. It was assumed that the jaws and symphseal membrane have the same density as water. As such, the lower jaw was modelled as two elliptic cylinders to account for the mandibular rami and a partial half ellipsoid to account for the mass of the sympyseal membrane and the water it puts into motion (Fig. 5). Mass and torque components of the individual rami incorporated in model were assumed to operate independently from (but additively to) the contralateral ramus. Under these conditions, the mass moment of inertia is described by:

$$I = I_{rami} + I_{sym},$$

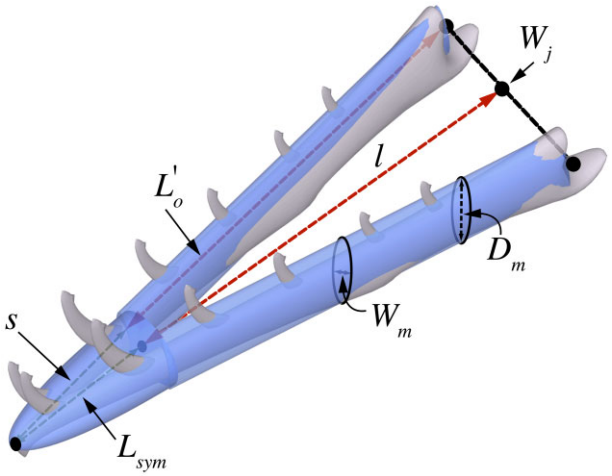

Figure 5. The strategy for modelling the mass of the jaw of loosejaw dragonfishes: shown in blue, a half ellipsoid of water for the symphyseal apparatus and as two elliptical cylinders for the partial length of the mandibular rami. L'_o, outlever length minus the lateral length of the symphseal apparatus (s); L_{sym}, length of symphyseal membrane; W_j, width of lower-jaw system at quadrato-articular joint; W_m, mandible width; D_m, mandible depth; l, computed distance from the axis of jaw rotation to the symphyseal membrane (i.e. $a - L_{sym}$); s, computed lateral width in partial half ellipse.

where I_{rami} is the mass moment of inertia of the mandibular rami (minus the symphyseal mass) and I_{sym} is the mass moment of inertia of the symphyseal apparatus. Thus, the mass moment of inertia of the two mandibular rami represented by two cylinders with the density of water is:

$$I_{rami} = 2\rho\pi\left(\frac{R_m^4 L'_o}{4} + \frac{R_m^2 L_o^3}{3}\right),$$

where R_m, L'_o, and ρ are the average radius of the mandible (i.e. average of W_m and D_m), length of the outlever minus the symphyseal apparatus, and the density of water (1000 g cm^{-3}), respectively. The mass moment of inertia of the half ellipsoid representing the symphyseal apparatus was expressed as a function of the distance x from the axis of rotation about the quadrato-articular joint:

$$I_{sym} = \pi\rho\int_l^a \frac{W_j^2}{4a^2}\sqrt{a^2 - x^2}\,x^3 dx,$$

where a is the length of the lower-jaw system from the centre of the of the axis of rotation about the quadrato-articular joint (i.e. $L_{sym} + l$) (Fig. 5), W_j is the width of the lower-jaw system at the joint, and l is the distance between the axis of rotation at the joint and the symphyseal membrane (i.e. $a - L_{sym}$)

(Fig. 5). The mass moment of inertia can thus be given by:

$$I_{sym} = \frac{W_j^2\sqrt{a^2-l^2}\,(2a^4+a^2l^2-3l^4)\pi\rho}{60a^2}.$$

Torque components

To calculate drag forces for the loosejaw species, *M. niger* and *A. scintillans*, the shape of the lower jaw was modelled as two elliptical cylinders and a half-elliptical plate with the same dimensions of the sagittal and coronal planes of the partial half ellipsoid. Under these conditions, the torque applied by drag forces was calculated using:

$$\tau_d = \tau_{d,rami} + \tau_{d,symp},$$

where $\tau_{d,rami}$ and $\tau_{d,sym}$ are the drag torques of the rami and symphyseal apparatus, respectively. Thus, the drag torque of the two mandibular rami represented by two elliptical cylinders is:

$$\tau_{d,rami} = -(1/4)\,\rho C_d W_m L_o'\omega^2,$$

where W_m and L_o are width of the mandible and inlever length, respectively, and ω is the angular velocity of the rotating jaw. The drag coeffecient was estimated from values given by Blevins (1984) for long elliptical cylinders and according to the aspect ratio of the lower jaw (i.e. D_m/W_m). The drag coefficient is a function of the Reynold's number (*Re*) and, for flow over a smooth cylinder, C_d declines sharply in the transition from laminar to turbulent ($Re > 10^5$) (Blevins, 1984). To attain this value, however, would require a velocity for loosejaw adduction approaching 25 m s^{-1}, a biologically unlikely scenario. Thus, it was assumed that flow over the elliptical cylinders of the mandibular rami occurred at relatively low *Re* values where C_d remains relatively independent of *Re*.

The drag torque of the symphseal membrane represented by a half elliptical plate was expressed as a function of the distance *x* from the axis of rotation about the quadrato-articular joint:

$$\tau_{d,sym} = \omega^2\rho C_d\left(\frac{W_j}{4a}\right)\int_l^a \sqrt{a^2-x^2}\,x^3dx.$$

With a coefficent of drag equal to 2.0, the value for flow normal to a flat plate (Blevins, 1984), the drag torque of the symphyseal membrane can thus be calculated by:

$$\tau_{d,sym} = \omega^2\rho W_j\left(\frac{\sqrt{a^2-l^2}\,(2a^4+a^2l^2-3l^4)}{30a}\right).$$

When the lower jaws of plesiomorphic species close, the intraoral volume will decrease, creating positive pressure that is exerted along the length of the lower jaw. Calculations of drag torques for *C. macouni* and *O. mitsuii*, assumed that oral pressures reached a peak of 200 pa (see 'Model alterations' in the Supporting information, Appendix S1). Because loosejaws lack a floor to the mouth, water passes by the mandibular rami during adduction and is therefore not trapped by the oral cavity. Thus, it was assumed that *A. scintillans* and *M. niger* do not produce supermabient pressures that would otherwise be caused by the compression of the oral cavity.

At each point in jaw-closing simulation, the torque applied to the lower jaw by the adductors is a function of the length of the inlever (i.e. distance of attachment point to the fulcrum of the quadrato-articular joint), angle of the lower jaw, and the force produced by the muscles. Muscle force calculations are performed *sensu* Van Wassenbergh *et al.* (2005) in which the maximum isometric force produced by the muscle (F_{max}), as determined by its physiological cross-sectional area, is scaled according to physiological parameters known to affect the contractile performance of vertebrate muscles, specifically:

$$F_{musc} = F_{max} \times F_{fv} \times F_{fl} \times F_{act} + F_{par}.$$

For details concerning calculations of F_{fv}, F_{fl}, F_{act}, and F_{par}, see the Supporting information (Appendix S1).

Jaw-closing simulations

Adduction simulations were performed with the model described above for each of the four stomiid species with biometric data isometrically scaled to a lower-jaw length of 30 mm (Table 1). Simulations were performed with a time step of 0.1 ms and iterated until the jaw was closed to a gape angle of 5°. At the beginning of jaw closing ($t = -0.1$ to $t = 0$ ms), jaw acceleration was set to 0 rad s^{-2}. To avoid circularity, at each time step, angular acceleration was computed based upon the values for the angular velocity and jaw angle from the previous time step ($t - 0.1$ ms). Gape angles for *M. niger* and *C. macouni* were set at 120° and 110°, respectively, according to the functional morphological analyses of Günther & Deckert (1959) and Tchernavin (1953). Because species of *Aristostomias* share extremely long jaws, lack of skin between the mandibular rami, similar muscle architecture, and a wide occipito-vertebral gap (Schnell *et al.*, 2010) with *Malacosteus*, it was assumed that

Table 1. Morphological data of the jaw-adduction system of the dragonfishes *Malacosteus niger, Aristostomias scintillans, Chauliodus macouni*, and *Opostomias mitsuii*

Species	SL	L_i	L_o	MA	W_j	W_m	D_m	L_{sym}	Muscle	*ML* (mm)	D_{oj} (mm)	Mass (mg)	θ (°)	Average *FL*	PCSA (cm^2)	F_{max} (N)
Malacosteus niger	121.2	2.2	28.2	0.076	6.0	0.39	1.8	6.0	A2	23.5	25.6	36.9	0	20.9	0.0334	0.07
									A3	10.1	11.7	3.0	9.9	8.9	0.0063	0.01
Aristostomias scintillans	120.1	2.5	28.7	0.087	6.4	0.77	2.8	6.6	A2	18.1	20.2	37.1	0	15.2	0.0462	0.09
									A3	17.5	19.7	9.3	11.0	8.9	0.0195	0.04
Chauliodus macouni	202.6	4.5	28.9	0.155	9.7	0.85	5.6	6.0	A2-Aω	20.3	22.7	261	0	17.9	0.274	0.55
									A3	11.9	12.7	36.9	12.2	8.4	0.081	0.16
Opostomias mitsuii	281.8	5.6	28.1	0.200	16.6	NA	NA	NA	A2-Aω	20.0	22.7	328	13.5	15.4	0.391	0.782
									A3	11.4	14.3	143	20.1	9.0	0.283	0.567

Data reported represent values for hypothetical specimens isometrically scaled to a jaw length of 30 mm. For a summary of raw data taken from individual specimens, see the Supporting information (Table S1). NA, not available.

SL, standard length; L_j, lower-jaw length; L_i, inlever length for both A2 and A3 insertions; L_o, outlever length for both A2 and A3 insertions; W_j, width at quadrato-articular joint; W_m, average width of the mandibular rami; D_m, average depth of the mandibular rami; M_j, mass of the lower jaw; *ML*, muscle length; D_{oj}, distance from the muscle origin to quadrato-articular joint; L_{sym}, length of the symphyseal membrane; PCSA, physiological cross-sectional area; F_{max}, maximum isometric force; θ, pennation angle; *FL*, muscle-fibre length.

A. scintillans deployed and retracted its lower jaw in a manner similar to *M. niger* as described by Günther & Deckert (1959). Thus, the gape angle for *A. scintillans* was also set at 120°. A gape angle of 90° was assumed for *O. mitsuii* based on the manipulation of preserved specimens.

Because physiological and morphological parameters such as adductor attachment site (i.e. inlever length) and physiological cross-sectional area (PCSA) affect the performance of jaw closing (Van Wassenbergh *et al*., 2005; de Schepper, Van Wassenbergh & Adriaens, 2008), it may be difficult to uncover the functional significance of the loosejaw condition when such parameters vary considerably between species. The biomechanical modelling approach taken in the present study allowed these parameters to be altered so that their effects on the performance of jaw adduction could be isolated from the effects of presence or absence of skin between the mandibular rami. Accordingly, a second round of simulations was performed for *C. macouni* and the loosejaw *M. niger* in which morphological and physiological parameters were constrained to match values of the other species. Alternative simulations for the plesiomorphic *C. macouni* included: (1) adduction without skin between the mandibular rami (i.e. the lower jaw was modelled as it would be for the loosejaw species but with morphological data for *C. macouni*) and (2) with inlever lengths producing a mechanical advantage (MA) of 0.09 (the shortest inlever allowed by the muscle architecture) to 0.32. For loosejaw simulations of *C. macouni*, the symphyseal membrane was made proportional to that of *M. niger*. Alternative simulations for the loosejaw *M. niger* included: (1) adduction with skin between (i.e. the lower jaw was modelled as it would be for the plesiomorphic species but with morphological data for *M. niger*); (2) with the lower jaw in the plesiomorphic condition and PCSAs of the adductors equal to both those of *C. macouni* and 100–1000% of their normal values for *M. niger*; (3) with an inlever length producing an MA equal to that of *C. macouni*; and (4) inlever lengths producing MAs of 0.07–0.16.

RESULTS

Muscle force and adduction dynamics

In all species, A2 was largest in terms of PCSA. As a proportion of A2, the PCSA of A3 was smallest in *M. niger* at approximately 20%, whereas the PCSA of A3 was largest in *O. mitsuii* at 73%. The total PCSA supplying force to jaw adduction was considerably smaller in the loosejaw species than in the non-loosejaw taxa. The total PCSAs of *M. niger* and *A. scintillans* were 0.040 and 0.066 cm^2, respectively,

whereas those of *C. macouni* and *O. mitsuii* were 0.355 and 0.674 cm^2, respectively (Table 1).

Lower-jaw adduction simulations demonstrated that, in all four stomiid species, the initial muscular torque is used to accelerate the mass of the lower jaw (i.e. overcome the mass moment of inertia; Fig. 6). After this phase, the dynamics of jaw closing were much different in loosejaw versus non-loosejaw taxa, a difference partly a result of the lack of a pressure torque in the loosejaw species. In the plesiomorphic species, after accelerating the mass of the lower jaw, drag was the most important force acting against the closing jaw for only a short phase: 20% and 15% of jaw closing in *C. macouni* and *O. mitsuii*, respectively (Fig. 6A, B). Pressure then becomes the greatest and most prolonged antagonistic force, lasting 55% of jaw adduction in *O. mitsuii* and 63% of adduction in *C. macouni* (Fig. 6A, B). In the loosejaws *M. niger* and *A. scintillans*, drag imposed a negative force much greater than the initial moment of interia for approximately the last three-quarters of adduction (Fig. 6C, D).

The models predicted closing durations of 89.1 ms and 103.0 for the loosejaws *A. scintillans* and *M. niger*, respectively, and 66.6 ms and 83.6 ms for the plesiomorphic species *O. mitsuii* and *C. macouni*, respectively (Table 2). Although the closing durations of the loosejaw species were slower than either of the plesiomorphic species, average closing velocities for all four dragonfishes were comparable, at 1.17 and 1.35 $^\circ\,ms^{-1}$ for *M. niger* and *A. scintillans*, respectively, and 1.31 and 1.35 $^\circ\,ms^{-1}$ for *C. maconi* and *O. mitsuii*, respectively (Table 2). The jaws of the plesiomorphic species were most powerful. The predicted maximal static bite force was 56.9×10^{-3} N for *O. mitsuii* and $37.6. \times 10^{-3}$ N for *C. macouni*. The loosejaw species *A. scintillans* and *M. niger* produced much smaller magnitudes of peak static bite forces of 4.6×10^{-3} N and 3.1×10^{-3} N, respectively (Table 2).

Alternative simulations

Simulated jaw adduction for *C. macouni* with skin absent between the mandibular rami (i.e. the lower jaw was modelled as it would be for a loosejaw, but with morphological data for *C. macouni*), the jaw closed in 58.3 ms, 30.3% faster than under plesiomorphic conditions (Fig. 7A; Table 3). Peak angular velocity increased by a slightly larger magnitude of 41.0%, to $2.60 \times 10^3\,^\circ\,s^{-1}$ and static bite force decreased 42.1% to 21.8×10^{-3} N (Fig. 7B, C; Table 3).

A series of simulations for *C. macouni* with a change to the attachment site of the adductors that produced MAs in the range 0.09–0.32 demonstrated that an increase in inlever length results in a decrease in adduction duration until an MA of 0.15, an increase in force until an MA of 0.20, and increased peak velocity (Fig. 8A, B, C). At all MA values, a phase of high force output was reached early, by approximately 10–20 ms; force then remains relatively steady until increasing steadily for the last half or more of adduction (Fig. 8D). Because of relatively high resistive forces over the last half of adduction (Fig. 6A), velocity decreases rapidly (Fig. 8E).

Simulations for *M. niger* under non-loosejaw conditions (i.e. as it would be for *C. macouni* or *O. mitsuii* but with morphological data from *M. niger*) predicted that the jaw could not overcome resistive forces and would stall at approximately 95° after 60 ms (Table 3). Under these same conditions but with PCSAs comparable to *C. macouni* (i.e. A2 and A3 PCSA increased 1200% and 820%, respectively), the jaw closed in 81.9 ms, 20.0% faster than under the normal loosejaw conditions (Table 3). Peak angular velocity increased 49.3% to $2.12 \times 10^3\,^\circ\,s^{-1}$, whereas maximum static bite force increased 677% to 24.1×10^{-3} N. A series of simulations in which the A2 and A3 PCSAs were each increased from 100% to 1000% predicted that *M. niger* with a mandibular

Table 2. Results of jaw-closing simulations for the deep-sea dragonfishes *Malacosteus niger, Aristostomias scintillans, Chauliodus macouni*, and *Opostomias mitsuii*

	Time (ms)	Maximum linear velocity at jaw tip ($cm\,s^{-1}$)	Maximum angular velocity ($10^3\,^\circ\,s^{-1}$)	Average angular velocity ($10^3\,^\circ\,s^{-1}$)	Peak bite force (10^{-3} N)
Malacosteus niger	103.0	71.1	1.42	1.17	3.1
Aristostomias scintillans	89.1	82.5	1.65	1.38	4.6
Chauliodus macouni	83.6	93.2	1.85	1.31	37.6
Opostomias mitsuii	66.6	90.4	1.85	1.35	56.9

Data reported are for simulations of hypothetical specimens with morphological parameters scaled isometrically to a lower-jaw length of 30 mm.

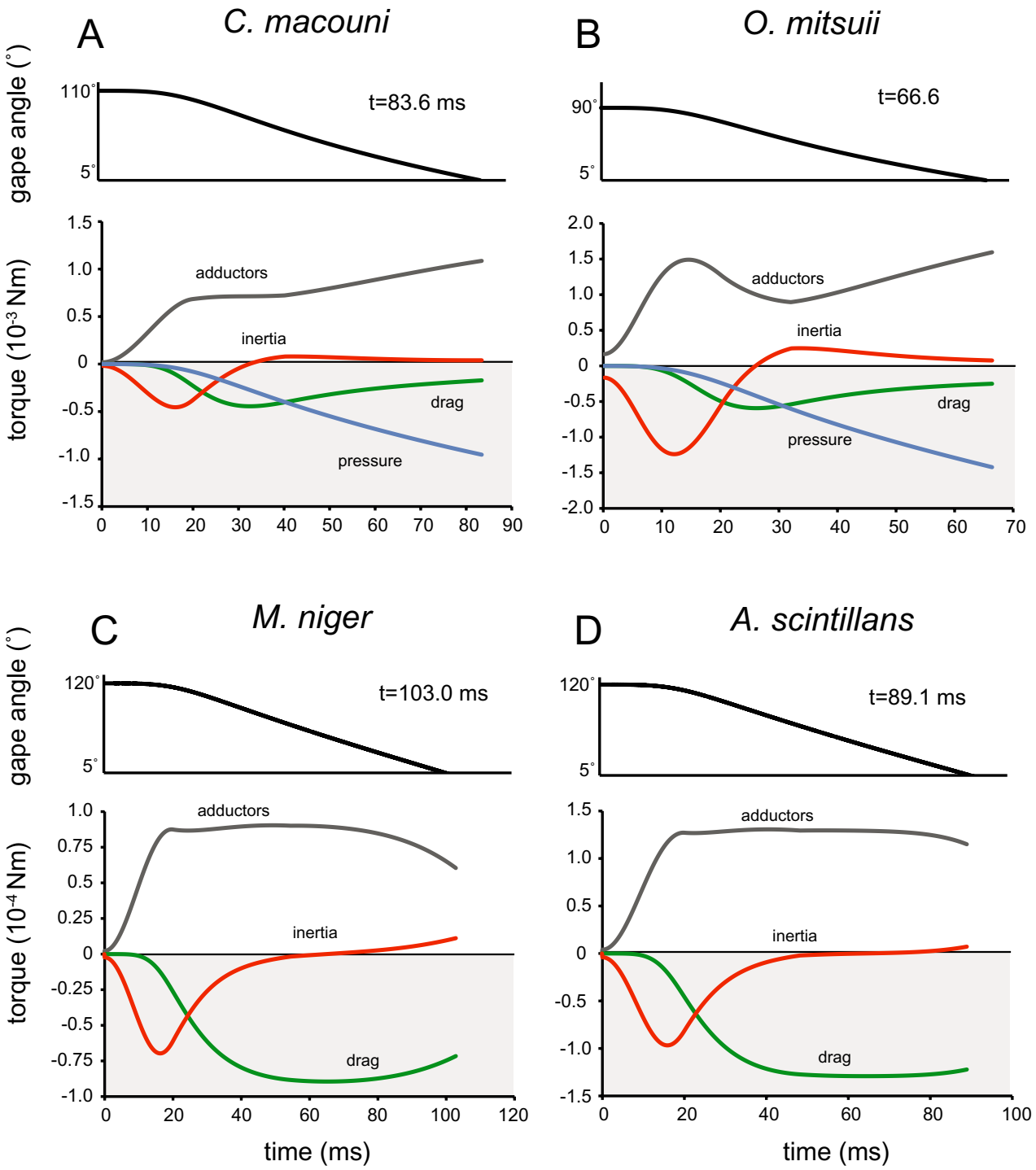

Figure 6. Model output of torques affecting lower-jaw adduction in four species of dragonfishes: A, *Chauliodus macouni*. B, *Opostomias mitsuii*. C, *Malacosteus niger*. D, *Aristostomias scintillans*. Positive values above the vertical line contributed to the acceleration of the lower jaw, negative values contributed to deceleration. Red line, inertia; black line, torque applied by the adductors; green line, drag; blue line, pressure.

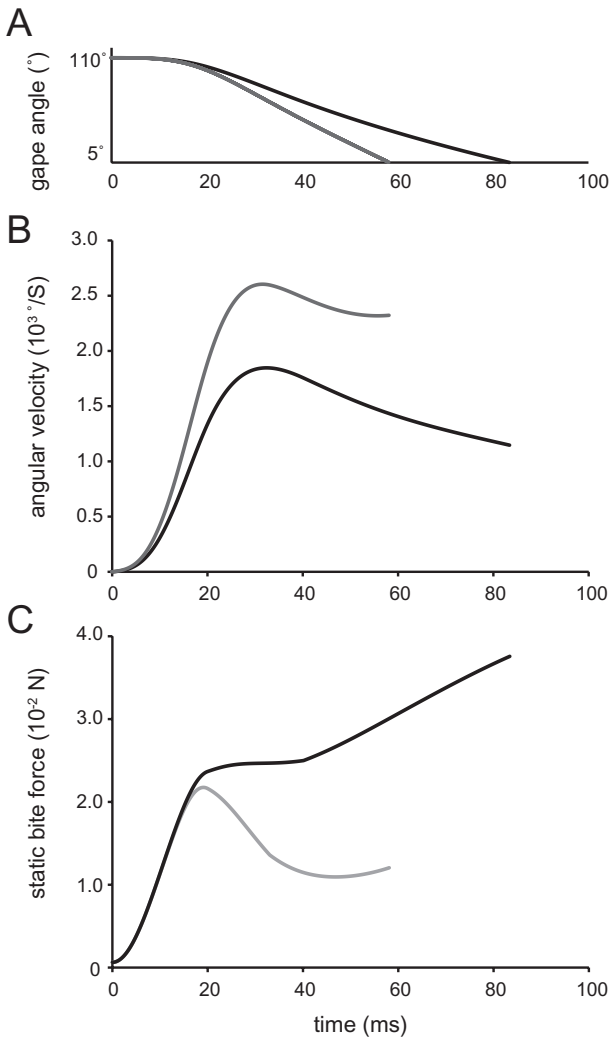

Figure 7. Model output of jaw angle (A), angular velocity (B), and static bite force at the tip of the lower jaw (C) during simulated adduction in *Chauliodus macouni*. Black line represents output for *C. macouni* under the plesiomorphic model (i.e. with a intermandibular membrane); grey line represents output under a loosejaw model (i.e. without a intermandibular membrane).

membrane would overcome resistive forces only after an increase of 800% (Fig. 9).

Simulations for *M. niger* with a MA of 0.155, that of *C. macouni*, predicted that the jaw would close in 122.7 ms, slower by 19.1%. Peak angular velocity and maximal static bite force were predicted to increase by 7.8% to 1.53×10^3 ° s^{-1} and 19.4% to 3.65×10^{-3} N, respectively (Table 3). Simulations increasing MA from 0.07 to 0.16 revealed that the jaw would close more slowly at both above and below an MA of 0.076 (Fig 9A). For these same simulations, maximal static bite force and peak angular velocity increased throughout the range of MAs (Fig. 10B, C). As the MA was increased, phases of force and velocity were achieved later in the jaw-closing cycle (Fig. 10D, E). Unlike in similar simulations for *C. macouni*, force does not increase sharply in the last half of jaw closing throughout the range of MA values but remains relatively static (Fig. 10D).

DISCUSSION

Model accuracy

The same computational models developed for clariid catfishes by Van Wassenbergh *et al*. (2005) produced rather accurate predictions of biting performance relative to laboratory observations for several aspects of lower-jaw adduction, including duration and peak angular velocity. Thus, it appears that a dynamic model of lower-jaw adduction can provide valuable insight into feeding behaviour of fishes and that the model predictions for stomiid dragonfishes may provide reasonable estimations of lower-jaw kinematics in these taxa. There is no doubt, however, that better estimates for several important model parameters may improve the accuracy of these dynamic models. Although some aspects of aquatic prey capture have been studied intensively, especially regarding how fishes create suction (Ferry-Graham & Lauder, 2001; Wainwright *et al*., 2007), the biomechanics and hydrodynamics of jaw adduction have remained largely unstudied. In particular, contractile properties of teleost adductor mandibulae and the magnitude of buccal pressure and tissue resistance remain poorly understood. For the plesiomorphic species, this limitation required that buccal pressure be crudely estimated based on data from distantly related taxa (see 'Model alterations' in the Supporting information, Appendix S1). Similarly, the contractile properties of the adductor mandibulae were based on results of experiments focusing on the physiology of axial musculature. That these important parameters are based on data from distantly related taxa and disparate morphological systems demonstrates that our current understanding of jaw adduction in fishes remains relatively superficial.

Dynamics of jaw adduction in dragonfishes

In the dragonfishes *O. mitsui* and *C. macouni*, force applied by the jaw adductors is opposed initially by a large inertial torque, followed by a rather substantial drag torque for a short period, before buccal pressure becomes the largest opposing torque for more than half of jaw closing. This pattern is very similar to that reported by de Schepper, Van Wassenbergh & Adriaens (2008) using an almost identical model for two trichiurid species, *Aphanopus carbo* Lowe and *Trichiurus lepturus* L. However, it is in sharp contrast to

Table 3. Results of jaw-closing simulations for the deep-sea dragonfish *Chauliodus macouni* and *Malacosteus niger* under several morphological scenarios

	Chauliodus macouni	*Malacosteus niger*		
	MA = 0.155	A2 and A3 PCSA of *M. niger*	A2 and A3 PCSA of *C. macouni*	MA = 0.155
	Loosejaw	Plesiomorphic	Plesiomorphic	Loosejaw
Time (ms)	58.3	∞	81.9	122.7
Peak linear velocity at jaw tip (cm s^{-1})	131.4	30.6	106.4	76.5
Peak angular velocity (10^3 ° s^{-1})	2.60	0.611	2.12	1.53
Peak bite force (10^{-3} N)	21.8	5.52	24.1	3.65

MA, mechanical advantage; PCSA, physiological cross-sectional area.

the kinematic profiles of fishes with much shorter jaws. Van Wassenbergh *et al*. (2005) reported that the adductors of clariid catfishes overcome rather modest inertial forces very quickly and then encounter buccal pressure as the major negative forces for the remainder of lower-jaw adduction. Unlike in dragonfishes and trichiurids, drag is a negligible negative force acting against the lower jaw of catfishes.

The kinematic profile for the two loosejaw species contrasts those of the two plesiomorphic dragonfishes: the trichiurids studied by de Schepper *et al*. (2008), and the short-jawed fishes modelled by Van Wassenbergh *et al*. (2005). Without buccal compression, the adductors of loosejaws must overcome drag as the only resistive force after the mass of lower jaw is accelerated. As buccal pressure increases throughout the compressive phase of feeding in other fishes, the jaw slows as it approaches the palate. However, in loosejaws, the jaw maintains relatively high velocities over the second half of adduction (Fig. 8E) and is thus subject to the exponential scaling of drag with this velocity. Because of this important dynamic and fact that the mandibular rami are exposed as they rotate through the water, the shape of each ramus is no doubt an important parameter affecting the amount of drag that resists closing. Therefore, it might be predicted that loosejaw species have jaw shapes that reduce drag, and thus increase the performance of the jaw-closing system. In fact, the mandibular widths of *M. niger* and *A. scintillans* are extremely thin (< 1 mm) and the transverse profile of the mandibles are tapered with a thinner dorsal edge and thicker ventral margin. Furthermore, if jaw-closing simulations are performed for *M. niger* with mandibular widths that approximate those of the plesiomorphic *C. macouni*, closing time increases and peak velocity decreases by approximately 5%.

An understanding of the importance of drag in limiting the performance of the loosejaw feeding permits additional interpretations of the functional significance of this unique morphology. The presence of a substantial symphyseal membrane on the distal section of the jaw (a structure that comprises approximately half the surface area of the lower-jaw system) may represent a trade-off between faster jaw performance and some unknown functional advantage that this apparatus imparts in the capture of prey. If the length of the symphyseal membrane of *M. niger* is reduced by half, closing time decreases by 21%, whereas peak velocity increases by 27%. Thus, it appears that this structure has some functional importance worthy of such a significant reduction in closing performance, perhaps as a somewhat rigid plate against which prey can be secured during rotation toward the oral cavity.

The findings of the present study, together with results reported by de Schepper *et al*. (2008), indicate that negative forces are much higher for long-jawed fishes compared to the negative forces encountered by short-jawed fishes. The positive relationship between longer jaws and resistive forces is expected and indeed predicted by the dynamic components of the models. With an increase in mandible length, these models predict an exponential increase in moment of inertia and drag and pressure torques. Despite these predictions, simulated lower-jaw adduction in these fishes is relatively fast, both in terms of peak angular velocity and duration. Thus, these models predict the existence of concomitant morphological mechanisms that mitigate increased negative forces in long-jawed fishes.

The bite forces generated by all four dragonfishes (but particularly the two loosejaws) are remarkably low compared to other species of predatory fishes modelled in similar studies (Westneat, 2003; Van Wassenbergh *et al*., 2005; de Schepper *et al*., 2008). The effective capture of prey with such small magnitudes of force may be enabled by the extremely sharp

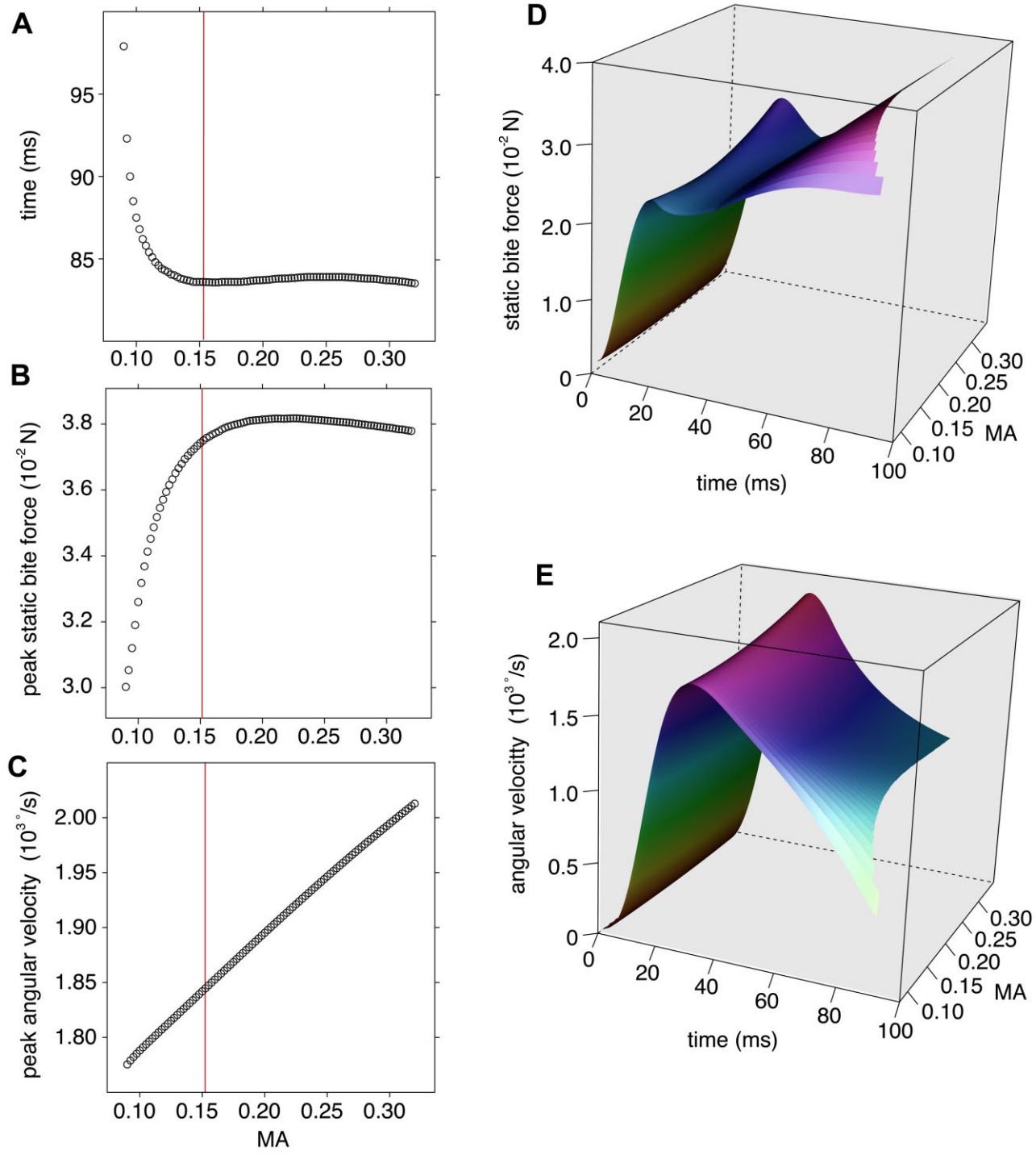

Figure 8. Model output of simulated lower-jaw adduction for *Chauliodus macouni* with mechanical advantage (MA) of 0.09–0.32: duration (A), static bite force (B), peak angular velocity (C), and static bite force and angular velocity throughout adduction (D and E, respectively). Vertical red lines in (A) to (C) represent the observed MA.

teeth of dragonfishes, structures which perhaps serve to concentrate bite force at their tips, and, in combination with quick adduction, permit a fast, piercing strike (for alternative interpretations, see also Günther & Deckert, 1959). Furthermore, this quick, piercing, but underpowered bite may be sufficient given the relatively soft bodies of most deep-sea taxa.

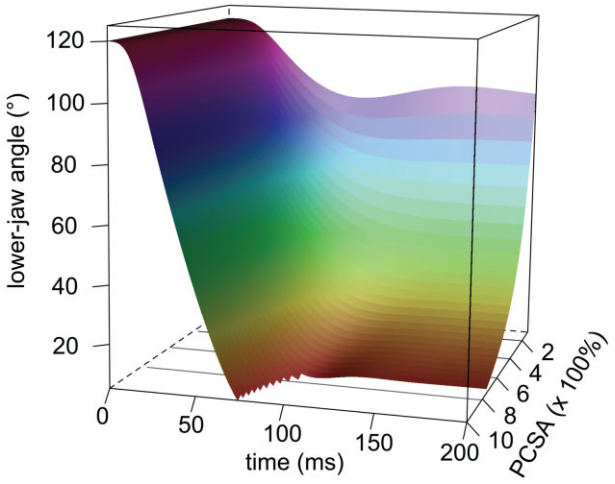

Figure 9. Model output of jaw angle versus duration in a simulated lower-jaw adduction for *Malacosteus niger* with an intermandibular membrane and with adductor physiological cross-sectional area (PCSA) in the range 100–1000% of normal.

Mechanical advantage and extremely long jaws

The enormous gapes and extremely long jaws of dragonfishes are no doubt important in capturing large and relatively fast prey items that comprise their diet (Clarke, 1982; Sutton & Hopkins, 1996). As other studies have shown (e.g. Ferry-Graham, Wainwright & Bellwood, 2001; Kammerer, Grande & Westneat, 2006), fishes with extremely long jaws must close their jaws quickly to capture relatively large elusive prey. Computing MA has often been used as a means to predict jaw-closing performance (Westneat, 1994; Grubich, Rice & Westneat, 2008; Maie, Schoenfuss & Blob, 2009). These and other studies have suggested that low inlever-outlever ratios (i.e. low MAs) facilitate relatively high jaw displacement and fast adduction at the expense of force transmission. The results of the present study suggest that, at least for fishes with extremely long jaws, caution is warranted when interpreting the functional relationship between MA and jaw-closing performance. In alternative simulations of adduction using a wide range of inlever lengths for the plesiomorphic *C. macouni*, adduction time unexpectedly decreased with an increase in MA from 0.09 to 0.15 (Fig. 8A), whereas both peak static bite force and angular velocity increase throughout the range of MA. In addition, phases of both high velocity and force transmission remained similarly long as MA was increased (Fig. 8C, D). As discussed above, the forces opposing jaw adduction in taxa with extremely long jaws, such as stomiids and trichiurid fishes, are of much higher magnitudes than fishes with shorter jaws. The results of the present study and others focusing on longer-jawed fishes suggest that the position of muscle insertion on the lower jaw of these species is constrained by relatively high resistive forces, especially drag and pressure, forces that scale exponentially with jaw length. In other words, fishes with extremely long jaws must have higher MA than fishes with shorter jaws, so that a greater force is transmitted to overcome the relatively higher resistive forces.

Functional significance of the loosejaw

Alternative simulations for *C. macouni* lacking skin between the mandibular rami demonstrate that, all else being equal, the loosejaw configuration improves closing performance considerably. The jaw closes 30.3% more quickly and increases peak angular velocity by 41% (Fig. 7). Based on these predictions, the innovation of the loosejaw apparatus in deep-sea dragonfishes is, in part, an adaptation for speed, for springing the trap-like jaw quickly toward or against a prey item, just as Günther & Deckert (1959) predicted. An increase in overall speed by 30% means the jaw may encounter the prey item that much faster, providing a considerable advantage if an elusive prey item is to be directed into the oral cavity.

Results of simulations for *M. niger* suggest that the loosejaw condition may also be a solution to the 'long-jaw' problem. The loosejaw species *M. niger* and *A. scintillans* not only attained jaw-closing velocities comparable to *C. macouni* and *O. mitsuii*, but also met drag torques lower by one order of magnitude (Fig. 6, Table 2). By reducing the surface area of the lower jaw, loosejaws eliminate or drastically reduce resistive forces that are a function of this parameter. Although *C. macouni* and *O. mitsuii* encounter much higher resistive forces and must therefore rely on MA to generate high angular velocities and to close the jaw quickly, the loosejaw condition has permitted the evolution of a more posterior insertion for the adductors and the high displacement advantage offered by low inlever-outlever ratios (i.e. low MA). Furthermore, it might be predicted that, as a result of the reduction of resistive forces, this innovation has permitted the evolution of high-performing, extremely elongate jaws, the longest among dragonfishes. Indeed, if the outlever of *C. macouni* is lengthened 65% to approximate the relative size of the lower jaw of *M. niger* (in terms of standard length), the closing duration increases by 400% to 333 ms. Without long and fast lower jaws, the trap-like like feeding behaviour of loosejaws, in which the jaw must spring shut through a field of 120° or more, would be ineffective in the capture of large, elusive, and especially scarce resources in the deep-sea.

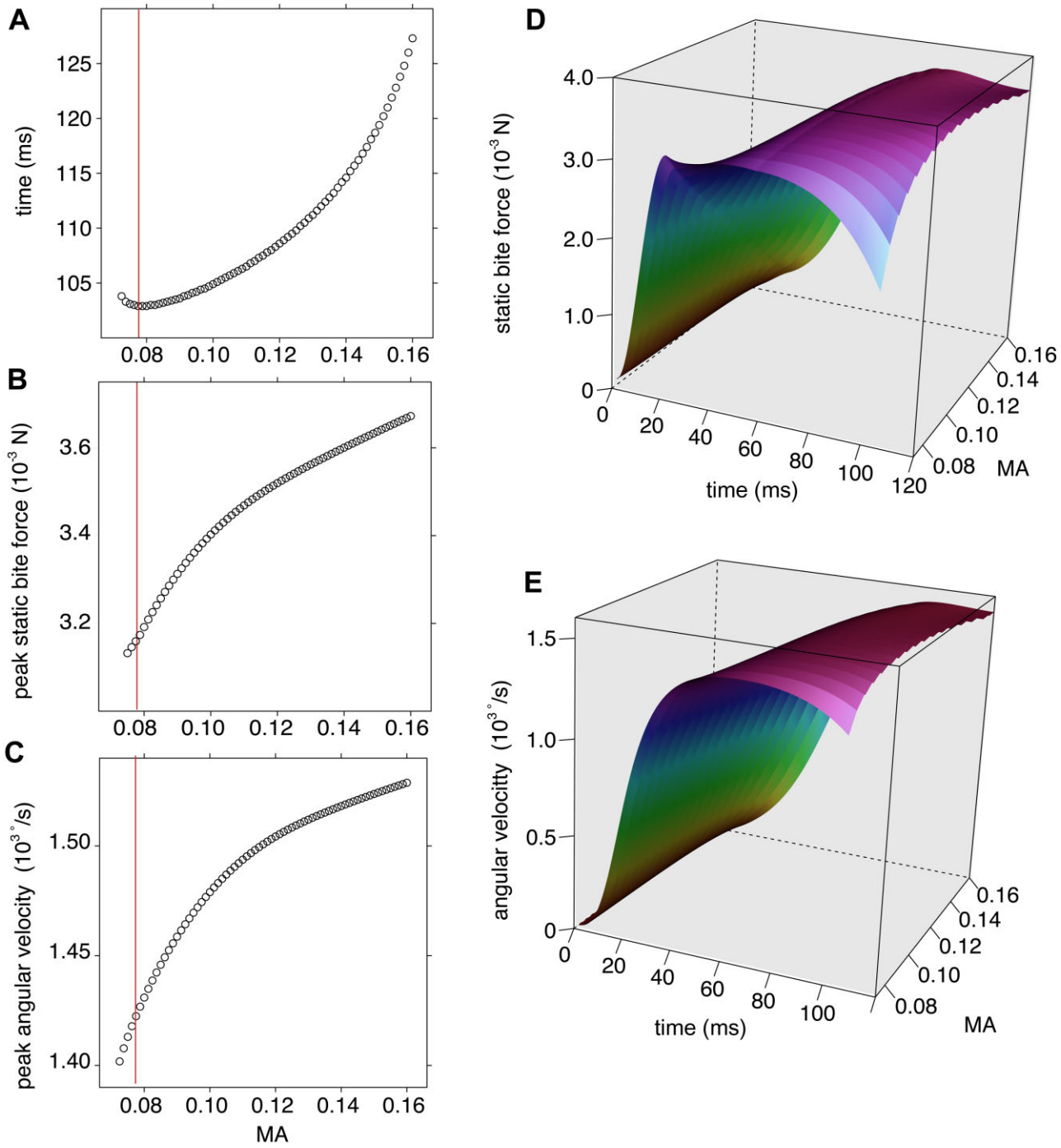

Figure 10. Model output of simulated lower-jaw adduction for *Malacosteus niger* with mechanical advantage (MA) of 0.07–0.16: duration (A), static bite force (B), peak angular velocity (C), and static bite force and angular velocity throughout adduction (D and E, respectively). Vertical red lines in (A) to (C) represent the observed MA.

It appears, however, that *M. niger* has reached the limits of this displacement advantage. In simulations with reduced inlever lengths (i.e. MAs lower than normal), adduction duration increases considerably (Fig. 10A). At these low MAs, phases of high force transmission are abbreviated with static bite force peaking early and decreasing steadily, and then precipitously toward the end of adduction (Fig. 10D).

Thus, at these low MAs, too little force is generated to counteract even the relatively minor forces resisting adduction.

The results of the present study also reveal, however, that this morphology is something more than an adaptation to reduce hydrodynamic drag that permits fast adduction with extremely elongate jaws. Simulations demonstrate that the loosejaw condition permits such weakly powered, extremely long jaws to close. With a mandibular membrane in place, the lower jaw of *M. niger* would not close. To close the jaw of *M. niger* with skin between the mandibular rami, the model predicts that A2 and A3 physiological cross-sectional areas would have to increase by over 800% (Fig. 9). From a bioenergetics perspective, the reduction of muscle volume permitted by the loosejaw condition would afford a considerable metabolic saving. An architectural solution to the long-jaw problem in the form of a loss of a mandibular membrane is an additional metabolic saving in itself.

ACKNOWLEDGEMENTS

I thank Karsten Hartel (MCZ) and Katherine Maslenikov (UW) for providing the material examined in the present study. Mark Westneat and Eric Ward provided insightful guidance and discussion, as did Theodore W. Pietsch, James W. Orr, and Courtney M. Peck, who also read an early version of the manuscript. Special thanks are extended to the three anonymous reviewers who made especially helpful comments and enhanced the quality of this contribution. This study was funded in part by the Dorothy T. Gilbert Memorial Endowment, University of Washington, Seattle.

REFERENCES

Alexander R. 2003. *Principles of animal locomotion*. Princeton, NJ: Princeton University Press.

Anderson P, Westneat M. 2007. Feeding mechanics and bite force modelling of the skull of *Dunkleosteus terrelli*, an ancient apex predator. *Biology Letters* **3:** 77–80.

Azizi E, Roberts TJ. 2010. Muscle performance during frog jumping: influence of elasticity on muscle operating lengths. *Proceedings of the Royal Society of London Series B, Biological Sciences* **277:** 1523–1530.

Blevins R. 1984. *Applied fluid dynamics handbook*. New York, NY: Van Nostrand Reinhold.

Carroll AM, Wainwright PC, Huskey SH, Collar DC, Turingan RG. 2004. Morphology predicts suction feeding performance in centrarchid fishes. *Journal of Experimental Biology* **207:** 3873–3881.

Clarke TA. 1982. Feeding habits of stomiatoid fishes from Hawaiian waters. *US Fishery Bulletin* **80:** 287–304.

Douglas RH, Partridge JC, Dulai KS, Hunt DM, Mullineaux CW, Hynninen PH. 1999. Enhanced retinal longwave sensitivity using a chlorophyll-derived photosensitiser in *Malacosteus niger*, a deep-sea dragon fish with far red bioluminescence. *Vision Research* **39:** 2817–2832.

Ferry-Graham L, Lauder G. 2001. Aquatic prey capture in ray-finned fishes: a century of progress and new directions. *Journal of Morphology* **248:** 99–119.

Ferry-Graham LA, Wainwright PC, Bellwood DR. 2001. Prey capture in long-jawed butterflyfishes (Chaetodontidae): the functional basis of novel feeding habits. *Journal of Experimental Marine Biology and Ecology* **256:** 167–184.

Fink WL. 1985. Phylogenetic interrelationships of the stomiid fishes (Teleostei: Stomiiformes). *Miscellaneous Publications Museum of Zoology University of Michigan* **171:** i–vii. 1–127.

Grubich J, Rice A, Westneat M. 2008. Functional morphology of bite mechanics in the great barracuda (*Sphyraena barracuda*). *Zoology* **111:** 16–29.

Günther K, Deckert K. 1959. Morphologie und Funktion des Keifer- und Kiemenapparates von Tiefseefishcen der Gattungen *Malacosteus* und *Photostomias* (Teleostei, Isospondyli, Stomiatoidea, Malacosteidae). *Dana Report* **49:** 1–54.

Higham TE, Day SW, Wainwright PC. 2006. The pressures of suction feeding: the relation between buccal pressure and induced fluid speed in centrarchid fishes. *Journal of Experimental Biology* **209:** 3281–3287.

Hill A. 1938. The heat of shortening and the dynamic constants of muscle. *Proceedings of the Royal Society of London Series B, Biological Sciences* **126:** 136–195.

Hunt DM, Dulai KS, Partridge JC, Cottrill P, Bowmaker JK. 2001. The molecular basis for spectral tuning of rod visual pigments in deep-sea fish. *Journal of Experimental Biology* **204:** 3333–3344.

James R, Cole N, Davies M, Johnston I. 1998. Scaling of intrinsic contractile properties and myofibrillar protein composition of fast muscle in the fish *Myoxocephalus scorpius* L. *Journal of Experimental Biology* **201:** 901–912.

Kammerer C, Grande L, Westneat M. 2006. Comparative and developmental functional morphology of the jaws of living and fossil gars (Actinopterygii: Lepisosteidae). *Journal of Morphology* **267:** 1017–1031.

Kenaley C, Hartel K. 2005. A revision of Atlantic species of *Photostomias* (Teleostei: Stomiidae: Malacosteinae), with a description of a new species. *Ichthyological Research* **52:** 251–263.

Kenaley CP. 2007. Revision of the stoplight loosejaw genus *Malacosteus* (Teleostei: Stomiidae: Malacosteinae), with description of a new species from the temperate southern hemisphere and Indian Ocean. *Copeia* **2007:** 886–900.

Kenaley CP. 2009. Revision of Indo-Pacific Species of the Loosejaw Dragonfish Genus *Photostomias* (Teleostei: Stomiidae: Malacosteinae). *Copeia* **2009:** 175–189.

Lauder GV. 1980. The suction feeding mechanism in sunfishes (*Lepomis*): an experimental analysis. *Journal of Experimental Biology* **88:** 49–72.

Maie T, Schoenfuss H, Blob R. 2009. Jaw lever analysis of Hawaiian gobioid stream fishes: a simulation study of

morphological diversity and functional performance. *Journal of Morphology* **270:** 976–983.

Narici M. 1999. Human skeletal muscle architecture studied in vivo by non-invasive imaging techniques: functional significance and applications. *Journal of Electromyography and Kinesiology* **9:** 97–103.

Partridge JC, Douglas RH. 1995. Far-red sensitivity of dragon fish. *Nature* **375:** 21–22.

Pietsch TW. 1978. The feeding mechanism of *Stylephorus chordatus* (Teleostei: Lampridiformes): functional and ecological implications. *Copeia* **1978:** 255–262.

Rasband W. 1997–2010. *ImageJ*. Bethesda, MD: National Institutes of Health.

Rassier D, MacIntosh B, Herzog W. 1999. Length dependence of active force production in skeletal muscle. *Journal of Applied Physiology* **86:** 1445–1457.

de Schepper N, Van Wassenbergh S, Adriaens D. 2008. Morphology of the jaw system in trichiurids: trade-offs between mouth closing and biting performance. *Zoological Journal of the Linnean Society* **152:** 717–736.

Schnell NK, Britz R, Johnson GD. 2010. New insights into the complex structure and ontogeny of the occipito-vertebral gap in barbeled dragonfishes (Stomiidae, Teleostei). *Journal of Morphology* **271:** 1006–1022.

Sutton TT, Hopkins TL. 1996. Trophic ecology of the stomiid (Pisces: Stomiidae) fish assemblage of the eastern Gulf of Mexico: strategies, selectivity and impact of a top mesopelagic predator group. *Marine Biology* **127:** 179–192.

Svanbäck R, Wainwright PC, Ferry-Graham LA. 2002. Linking cranial kinematics, buccal pressure, and suction feeding performance in largemouth bass. *Physiological and Biochemical Zoology* **75:** 532–543.

Tchernavin V. 1953. *The feeding mechanisms of a deep sea fish,* Chauliodus sloani *Schneider*. London: British Museum of Natural History.

Van Leeuwen J, Muller M. 1982. The recording and interpretation of pressures in prey-sucking fish. *Netherlands Journal of Zoology* **33:** 425–475.

Van Wassenbergh S, Aerts P, Adriaens D, Herrel A. 2005. A dynamic model of mouth closing movements in clariid catfishes: the role of enlarged jaw adductors. *Journal of Theoretical Biology* **234:** 49–65.

Wainwright P, Carroll AM, Collar DC, Day SW, Higham TE, Holzman RA. 2007. Suction feeding mechanics, performance, and diversity in fishes. *Integrative and Comparative Biology* **47:** 96–106.

Ward SR, Lieber RL. 2005. Density and hydration of fresh and fixed human skeletal muscle. *Journal of Biomechanics* **38:** 2317–2320.

Westneat M. 1994. Transmission of force and velocity in the feeding mechanisms of labrid fishes (Teleostei, Perciformes). *Zoomorphology* **114:** 103–118.

Westneat M. 2003. A biomechanical model for analysis of muscle force, power output and lower jaw motion in fishes. *Journal of Theoretical Biology* **223:** 269–281.

Westneat M. 2004. Evolution of levers and linkages in the feeding mechanisms of fishes. *Integrative and Comparative Biology* **44:** 378–389.

Whiting B, Herzog W. 1999. *Theoretical models of skeletal muscle: biological and mathematical considerations*. Chichester: Wiley.

Winterbottom R. 1974. A descriptive synonymy of the striated muscles of the Teleostei. *Proceedings of the Academy of the Natural Sciences of Philadelphia* **125:** 225–317.

Woittiez R, Huijing P, Boom H, Rozendal R. 1984. A three-dimensional muscle model: a quantified relation between form and function of skeletal muscles. *Journal of Morphology* **182:** 95–113.

SUPPORTING INFORMATION

Additional Supporting Information may be found in the online version of this article:

Appendix S1. List of material examined and detailed explanation of model construction.
Table S1. Morphological data of the jaw-adduction system from four specimens each of the dragonfishes *Malacosteus niger, Aristostomias scintillans, Chauliodus macouni*, and *Opostomias mitsuii*. Data are reported as range (mean ± SD). All measurements are in millimetres, unless otherwise noted. For further explanation of measurements, see Figures 1 and 2.

Please note: Wiley-Blackwell are not responsible for the content or functionality of any supporting materials supplied by the authors. Any queries (other than missing material) should be directed to the corresponding author for the article.